Asian Journal of Current Research in Clinical Cancer
ISSN: 3062-4444
2025, Volume 5, Issue 1, Page No: 177-195

Available online at: www.galaxypub.co/page/journals

Galaxy Publication

Galaxy Publication

The Alternative Splicing of CLSTN1 Driven by ESRP1 Suppresses Gastric Cancer Metastasis

Emily Fernandez[1]*, Mei Q. Moore[1]

[1]Department of Clinical Oncology, School of Medicine, Trinity College Dublin, Dublin, Ireland.

***E-mail** ✉ efernandez@outlook.com

Received: 15 January 2025; **Revised:** 09 March 2025; **Accepted:** 11 March 2025

ABSTRACT

The spread of tumors significantly worsens outcomes for individuals with gastric cancer. RNA-binding proteins (RBPs) play key roles in cancer spread, although their specific contributions to gastric cancer remain underexplored. In this work, we identified ESRP1, an epithelial-specific RBP, as a critical modulator of metastatic behavior in gastric cancer cells. Levels of ESRP1 show an inverse association with both distant and lymph node metastases in affected patients. Experiments confirmed that ESRP1 suppresses cell migration and invasion in gastric cancer models both in laboratory settings and animal studies. At the molecular level, ESRP1 facilitates alternative splicing of exon 11 in CLSTN1 pre-mRNA. The resulting shorter isoform of CLSTN1 strengthens the interaction between E-cadherin and β-catenin, while enhancing ubiquitination and subsequent degradation of β-catenin protein, ultimately restraining migratory and invasive properties of gastric cancer cells. This investigation underscores ESRP1's suppressive influence on gastric cancer spread and uncovers additional mechanistic insights. Findings suggest that ESRP1 and CLSTN1 could serve as promising targets for interventions against metastatic gastric cancer.

Keywords: Metastasis, Gastric cancer, CLSTN1, ESRP1

How to Cite This Article: Fernandez E, Moore MQ. The Alternative Splicing of CLSTN1 Driven by ESRP1 Suppresses Gastric Cancer Metastasis. Asian J Curr Res Clin Cancer. 2025;5(1):177-95. https://doi.org/10.51847/cZOZ2TW0T4

Introduction

Gastric cancer ranks among the leading malignant diseases globally, with over one million new cases annually, accounting for 5.6% of total cancer incidences [1, 2]. Its insidious development and nonspecific early symptoms often lead to diagnosis at advanced stages, frequently involving locoregional invasion or remote spread [3]. Metastasis represents the primary determinant of poor prognosis in gastric cancer, where five-year survival reaches up to 70% in early-stage disease but drops below 30% in advanced cases [4]. Therefore, identifying metastasis-associated factors and elucidating their roles and underlying pathways could advance therapeutic strategies and improve patient outcomes.

RNA-binding proteins (RBPs) form a highly conserved family equipped with domains for RNA interaction [5, 6]. They constitute approximately 10% of protein-encoding genes [7] and govern processes such as alternative splicing, mRNA stability, transport, and localization, thereby contributing to genomic variability and integrity [8–10]. Research indicates that dysregulated RBPs drive oncogenesis and tumor advancement, affecting cell growth, epithelial-mesenchymal transition (EMT), and other events via control of pre-mRNA splicing [11–13].

Epithelial splicing regulatory protein 1 (ESRP1) functions as an epithelial-restricted RNA-binding protein and splicing regulator essential for preserving epithelial traits and modulating cancer progression [14, 15]. Existing evidence reveals inconsistent effects of ESRP1 across malignancies: it acts protectively in some while promoting disease in others. For instance, higher ESRP1 levels correlate with better prognosis in pancreatic cancer, where overexpression markedly reduces hepatic spread [16]. In lung adenocarcinoma, ESRP1 curbs invasion and metastasis through EMT modulation [17]. Conversely, ESRP1 exhibits oncogenic properties in breast cancer,

associating with reduced survival and enhanced lung metastasis in models [18]. Pro-metastatic actions of ESRP1 have also emerged in ovarian and prostate cancers [19, 20]. In gastric cancer, prior work noted that low ESRP1 expression in 85% of cases links to diffuse-type disease [21], which favors lymph node and peritoneal dissemination owing to weakened cell adhesions and yields dismal outcomes. Additionally, ESRP1-mediated isoform shifts in LRRFIP2 may impede gastric cancer metastasis [22].

Here, we investigated ESRP1's contributions to gastric cancer and its regulatory pathways. We observed inverse correlations between ESRP1 levels and lymph node involvement, distant spread, as well as TNM staging in patients. Further experiments revealed ESRP1 binding to CLSTN1 mRNA, driving exon 11 splicing. The truncated CLSTN1 variant counteracts EMT in gastric cancer cells, interacts with β-catenin to reinforce cytoskeletal integrity, and blocks cell motility and invasiveness. These data reinforce ESRP1's link to reduced metastatic potential in gastric cancer, revealing a new CLSTN1-dependent pathway for invasion and dissemination. This positions ESRP1 and CLSTN1 as viable candidates for targeted therapies in gastric cancer.

Materials and Methods

Cell Lines and clinical specimens

Human gastric cancer cell lines SGC7901, BGC823, AGS, and MKN45 were acquired from the National Collection of Authenticated Cell Cultures (China). These lines were maintained in RPMI-1640 medium (Gibco) containing 10% fetal bovine serum (FBS; Gibco). The human embryonic kidney cell line HEK293T, also sourced from the same collection, was grown in high-glucose Dulbecco's Modified Eagle's Medium supplemented with 10% FBS. All cultures were incubated at 37°C in a humidified atmosphere with 5% CO_2.

Resected gastric cancer tissues from 24 consecutive patients were collected from the Department of Gastrointestinal Surgery, Union Hospital, Tongji Medical College, Huazhong University of Science and Technology. Informed written consent was obtained from all participants, and the protocol was approved by the Ethics Committee of Union Hospital, Tongji Medical College, Huazhong University of Science and Technology, in accordance with the Declaration of Helsinki (approval no. IEC-J-349).

Lentiviral constructs and transfection

Lentiviral vectors for overexpression of ESRP1, full-length CLSTN1 (CLSTN1-F), or truncated CLSTN1 (CLSTN1-S), as well as for knockdown of ESRP1 or CLSTN1-S, were obtained from Genechem (Shanghai). Stable cell lines with the desired overexpression and/or knockdown were established through lentiviral transduction followed by puromycin selection, per the manufacturer's guidelines.

Transwell migration and invasion assays

For migration assays, cells in logarithmic growth phase were collected and resuspended in RPMI-1640 medium with 2% FBS. A volume of 400 μL containing 1.2×10^5 cells was seeded into the upper chamber of a Transwell insert (Corning), while 500 μL of medium with 10% FBS was placed in the lower chamber of a 24-well plate. After 18 hours of incubation, inserts were fixed in 4% paraformaldehyde for 20 minutes, stained with crystal violet for 30 minutes, rinsed gently, and air-dried. Migrated cells on the underside of the membrane were enumerated under a microscope.

For invasion assays, the extracellular matrix was mimicked using Matrigel (#354248). Matrigel, thawed overnight at 4°C, was diluted 1:3 with ice-cold Opti-MEM (Gibco). 165 μL of diluted Matrigel was added to the upper chamber and polymerized at 37°C for 30 minutes; excess was carefully removed. Log-phase cells were resuspended at 1.5×10^5 cells per 400 μL in RPMI-1640 with 2% FBS and loaded into the coated upper chamber. The lower chamber received 500 μL of medium containing 10% FBS. Following 24 hours of incubation at 37°C, invaded cells on the membrane underside were fixed, stained, and quantified microscopically.

Western blotting and immunoprecipitation

Total cellular protein was isolated using RIPA lysis buffer (#R0278, Sigma) supplemented with protease inhibitor cocktail (#B14001, Biomake). Protein concentrations were determined with a BCA assay kit (#P0012, Beyotime). Samples were denatured by boiling in loading buffer (#P0015, Beyotime) for 10 minutes, resolved by sodium dodecyl sulfate–polyacrylamide gel electrophoresis (SDS-PAGE), and transferred to polyvinylidene fluoride membranes (Millipore). Membranes were blocked in 5% skim milk for 30 minutes at room temperature, then

probed with primary antibodies overnight at 4°C. After washing, membranes were incubated with horseradish peroxidase-conjugated secondary antibodies for 1 hour at room temperature. Signals were visualized using ECL reagents (#6883, Cell Signaling Technology) on an Invitrogen iBright CL1500 system (Thermo Fisher Scientific). Primary antibodies included: anti-ESRP1 (21045-1-AP, Proteintech, 1:1000), anti-E-cadherin (#14472, Cell Signaling Technology, 1:1000), anti-N-cadherin (#13116, Cell Signaling Technology, 1:1000), anti-CLSTN1 (12788-1-AP, Proteintech, 1:1000), anti-GAPDH (#60004–1-Ig, Proteintech, 1:3000), anti-β-catenin (#A19657, Abclonal, 1:1000). Secondary antibodies were HRP-conjugated goat anti-rabbit IgG H&L (#511203, ZENBIO, 1:3000) and goat anti-mouse IgG H&L (#511103, ZENBIO, 1:3000).

For immunoprecipitation, cells were lysed and protein quantified. Primary antibody was added to the lysate and incubated overnight at 4°C with rotation. Protein A/G magnetic beads or anti-Flag magnetic beads were then added for an additional 4-hour incubation at 4°C. Beads were washed, eluted by boiling in loading buffer, and analyzed by SDS-PAGE. The anti-β-catenin antibody (#A19657, Abclonal, 1:300) was used for IP, with rabbit IgG (#A7016, Beyotime) serving as isotype control.

Ni-NTA pulldown assay

β-catenin ubiquitination was assessed via Ni-NTA pulldown. His-tagged ubiquitin and Flag-tagged ESRP1, CLSTN1-F, or CLSTN1-S constructs were generated. Relevant plasmids were co-transfected into HEK293T cells. After 48 hours, cells were treated with 50 μM MG132 for 4 hours, harvested, and washed with PBS. Lysis was performed in urea buffer (8 M urea, 0.1 M NaH_2PO_4, 300 mM NaCl, 0.01 M Tris-HCl, pH 8.0), followed by brief sonication. A portion of lysate was retained as input; the remainder was incubated with Ni-NTA agarose beads (HY-K0210, MCE) for 2 hours at room temperature with rotation. Beads were washed five times with urea buffer, eluted by boiling in loading buffer for 10 minutes, and subjected to SDS-PAGE alongside input samples for detection.

PCR and agarose gel electrophoresis

Total RNA from gastric cancer cells or clinical tissues was isolated using RNAiso Plus (#9109, Takara) and reverse-transcribed with PrimeScript RT Master Mix (#RR036A, Takara). ESRP1 mRNA levels were quantified by real-time PCR using TB Green Premix Ex Taq II (#RR820A, Takara) on a StepOnePlus system (Thermo Fisher Scientific). Relative expression was calculated via the comparative Ct method ($2^{-\Delta\Delta Ct}$).

To detect the two CLSTN1 isoforms (CLSTN1-F and CLSTN1-S), primers flanking exon 11 were designed. Reverse-transcribed RNA from gastric cancer specimens was amplified using the Takara TP600 PCR system (Takara). Amplification products were resolved by agarose gel electrophoresis, and bands were visualized with TS-GelRed nucleic acid gel dye (TSJ003, Tsingke) on an Invitrogen iBright CL1500 imaging system (Thermo Fisher Scientific). Band intensities were quantified using ImageJ to determine grayscale values, and the splicing ratio was computed as the proportion of the short isoform relative to the total. Correlations between CLSTN1 splicing ratio and ESRP1 mRNA expression, lymph node metastasis status, or lymph node ratio (LNR; positive lymph nodes divided by total dissected lymph nodes) were evaluated.

In vivo tail vein injection metastasis assay

Metastatic capacity of gastric cancer cells was assessed in vivo via tail vein injection. Four-week-old BALB/c nude mice were obtained from HUAFUKANG Bioscience. Animals were randomly allocated to groups (n = 5 per group). SGC7901 (1.0×10^6) or MKN45 (1.5×10^6) cells suspended in 100 μL phosphate-buffered saline (PBS) were administered intravenously through the tail vein. After 1.5 months, mice were humanely euthanized, and lungs were harvested. Lungs were fixed overnight in Bouin's fixative at 4°C, dehydrated in 70% ethanol, and embedded in paraffin. Experiments were performed in a double-blinded manner, with injectors and evaluators unaware of group assignments. All procedures were approved by the Ethics Committee of Union Hospital, Tongji Medical College, Huazhong University of Science and Technology, and adhered to Institutional Animal Care and Use Committee guidelines (approval no. 3256).

Histology and immunohistochemistry (IHC)

Paraffin-embedded lungs were sectioned at 5–6 μm thickness. Hematoxylin and eosin (H&E) staining was performed using standard protocols to verify metastatic lesions and examine microscopic features. For IHC, sections were deparaffinized in xylene, rehydrated through graded ethanol, and endogenous peroxidase activity

was quenched. Antigen retrieval was followed by blocking nonspecific sites with 5% bovine serum albumin. Sections were incubated with anti-E-cadherin antibody (#14472, Cell Signaling Technology, 1:200) for 1 hour at 37°C, then with secondary antibody, and developed using the SABC kit (#SA1054, Boster Biological Technology) per the manufacturer's protocol.

RNA sequencing

Transcriptome analysis was performed on SGC7901 cells stably transduced with vector control or ESRP1 overexpression constructs. RNA was extracted from 1×10^7 cells, and library preparation with subsequent sequencing was outsourced to BGI.

Cross-linking immunoprecipitation (CLIP) sequencing

CLIP-seq was carried out by Ablife Institute (Wuhan). In brief, oeESRP1 SGC7901 cells were UV-crosslinked at 400 mJ/cm². Cells were lysed in ice-cold buffer (1× PBS, 0.1% SDS, 0.5% NP-40, 0.5% sodium deoxycholate) supplemented with 200 U/mL RNase inhibitor (Takara) and protease inhibitor cocktail (Roche), then incubated on ice for 30 minutes. Following centrifugation, RQ1 DNase (Promega) was added to the supernatant at 1 U/μL and incubated at 37°C for 30 minutes, after which digestion was halted with stop solution. The lysate was vigorously mixed, cleared by centrifugation at 13,000 × g for 20 minutes at 4°C, and subjected to limited RNA fragmentation with MNase (Thermo Fisher Scientific).

For immunoprecipitation, cleared supernatant was incubated overnight at 4°C with 10 μg anti-Flag antibody (#14793, Cell Signaling Technology) or control IgG (#2729, Cell Signaling Technology). Immune complexes were captured on protein A/G Dynabeads (Thermo Scientific) for 2 hours at 4°C. Beads were washed twice each with lysis buffer, high-salt buffer (250 mM Tris pH 7.4, 750 mM NaCl, 10 mM EDTA, 0.1% SDS, 0.5% NP-40, 0.5% deoxycholate), and PNK buffer (50 mM Tris, 20 mM EGTA, 0.5% NP-40). Bound material was eluted in buffer (50 mM Tris pH 8.0, 10 mM EDTA, 1% SDS) by heating at 70°C for 20 minutes with vortexing. After bead removal, Proteinase K (Roche) was added to both input (1%) and eluted samples at 1.2 mg/mL final concentration and incubated at 55°C for 120 minutes. RNA was purified using RNAiso Plus (#9109, Takara). Libraries were constructed with the KAPA RNA HyperPrep Kit (#KK8541, KAPA) following the manufacturer's instructions and sequenced on an Illumina NovaSeq platform for 150 nt paired-end reads.

RNA immunoprecipitation (RIP)-PCR

RIP was performed with slight adaptations from established protocols [23, 24]. In brief, 3×10^7 oeESRP1 SGC7901 cells were collected and rinsed twice with PBS. Lysis was carried out in polysome lysis buffer supplemented with protease inhibitor cocktail and RNase inhibitor. After DNase treatment to eliminate genomic DNA, 10% of the lysate was reserved as input, while the remainder was incubated overnight at 4°C with anti-ESRP1 antibody on a rotary shaker. Protein A/G magnetic beads were then added, and incubation continued for 2 hours. Beads were washed five times with wash buffer, and bound RNA was isolated using RNAiso Plus (#9109, Takara), followed by reverse transcription with PrimeScript RT Master Mix (#RR036A, Takara). The specific CLSTN1 mRNA region interacting with ESRP1 was confirmed by PCR amplification.

Bioinformatic analysis

To identify RNA-binding proteins (RBPs) associated with gastric cancer metastasis, two paired datasets comprising primary tumors, adjacent non-cancerous tissues, and metastatic lesions (GSE191139 and GSE206329) were retrieved from the Gene Expression Omnibus (GEO) database. Data normalization and processing were performed using the "affy" package in R version 4.0.0. Differential expression analysis between primary and distant metastatic samples was conducted with the "limma" package, and heatmaps were generated using the "pheatmap" package. Venn diagrams were employed to intersect and visualize RBPs within the differentially expressed genes (DEGs).

The association between ESRP1 expression and distant metastasis (M stage) in stomach adenocarcinoma patients from The Cancer Genome Atlas (TCGA) was evaluated via cBioPortal [25], with a Z-score threshold of 1.2. The impact of ESRP1 levels on progression-free survival in gastric cancer was assessed using Kaplan–Meier Plotter [26], with differences compared by log-rank test. The prognostic significance of CLSTN1 exon 11 alternative splicing in gastric cancer was examined using SpliceSeq data [27] accessed through the OncoSplicing database [28].

Statistical analysis

All statistical analyses were performed using GraphPad Prism 9.0 (GraphPad Software, Inc., La Jolla, CA). Data are presented as mean ± standard deviation (SD). Two-group comparisons of normally distributed data employed Student's t-test, whereas non-parametric data were analyzed with the Mann–Whitney test. Differences across multiple groups were evaluated by one-way ANOVA. Correlations involving ESRP1 expression, CLSTN1 splicing ratios, and metastatic parameters were assessed using Pearson correlation coefficient. Statistical significance was defined as a two-tailed $P < 0.05$.

Results and Discussion

ESRP1 shows inverse association with metastatic progression in gastric cancer

Analysis of two publicly available cohorts (GSE191139 and GSE206329) involved comparing transcriptional profiles between metastatic and non-metastatic gastric cancer samples. A heatmap displayed the 80 most differentially expressed genes (both increased and decreased) **(Figure 1a).** Subsequent screening based on magnitude of change and false discovery rate identified key candidates **(Figure 1b).** Among these, 40 RBPs exhibited upregulation in metastatic tumors, whereas 11, including ESRP1, demonstrated higher abundance in non-metastatic cases **(Figure 1c).** Validation using TCGA data via cBioPortal, incorporating expression and distant metastasis status for stomach adenocarcinoma, revealed markedly reduced ESRP1 in cases with remote spread (M1, n=7) compared to those without (M0, n=27) **(Figure 1d),** supporting an anti-metastatic role. Kaplan–Meier curves from the KM-plotter resource indicated better overall survival for patients with elevated ESRP1 (HR=0.66, 95% CI 0.52–0.84, P<0.001) **(Figure 1e).** In an independent cohort of 24 resected gastric cancer specimens, ESRP1 levels were notably higher in lymph node-negative versus node-positive disease **(Figure 1f).** Correlation analyses further linked lower ESRP1 to elevated lymph node ratio (LNR), a metric of nodal involvement **(Figure 1g).** Collectively, these observations position ESRP1 as a suppressor of metastatic dissemination in gastric cancer.

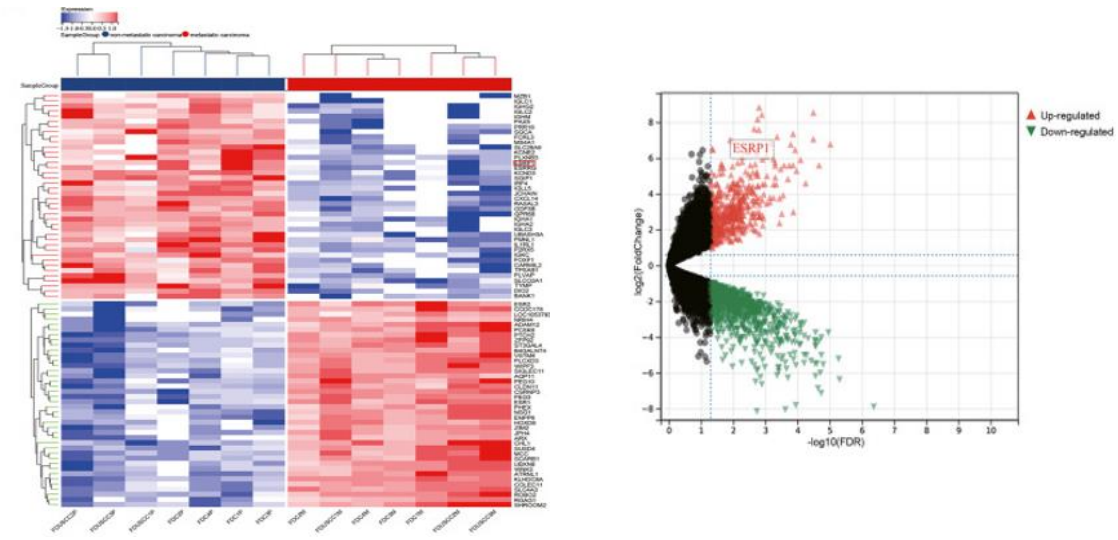

a) b)

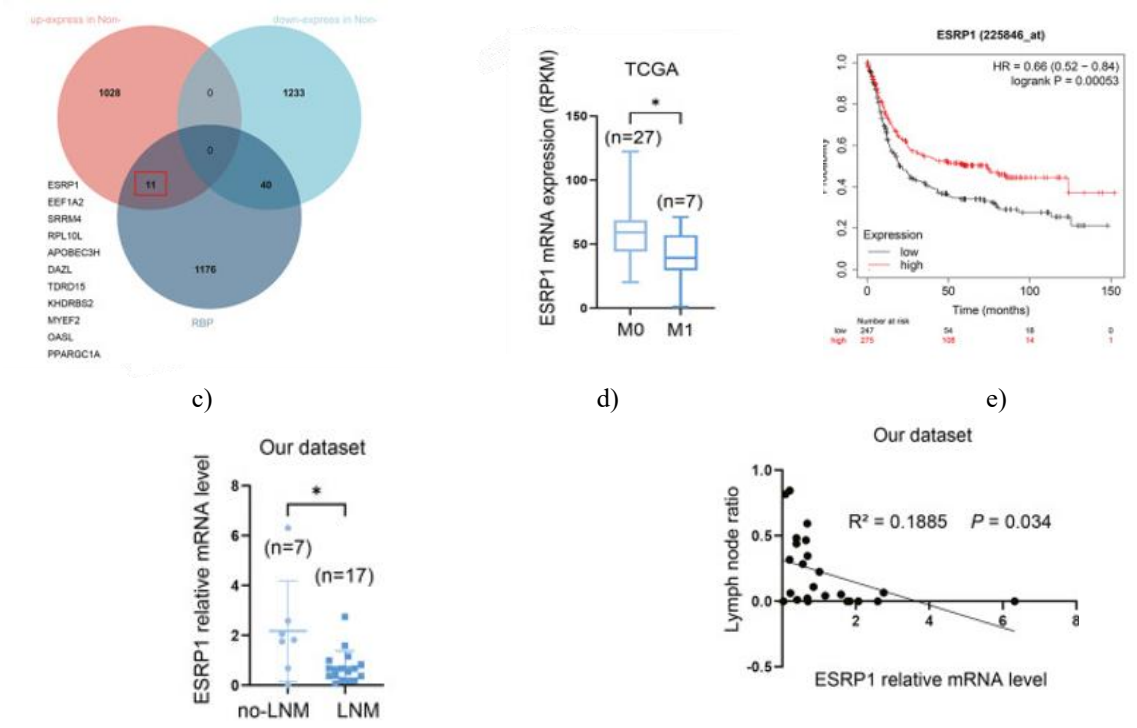

c) d) e)

f) g)

Figure 1. The RNA-binding protein ESRP1 exhibits reduced expression in gastric cancer cases with metastasis. a) Transcriptional profiles from the two cohorts (GSE191139 and GSE206329) were examined by categorizing samples into primary tumors (without metastasis) and those with metastatic involvement. A heatmap illustrates the leading upregulated and downregulated differentially expressed genes (DEGs), with color intensity reflecting relative expression levels.
b) Volcano plot depicting significantly upregulated and downregulated DEGs, with ESRP1 highlighted.
c) Differentially expressed RNA-binding proteins (RBPs) were pinpointed, and the 11 RBPs showing elevated expression in non-metastatic gastric cancer cases are enumerated.
d) Comparison of ESRP1 levels in stomach adenocarcinoma cases with distant metastasis (M1, n=7) versus without (M0, n=27), based on TCGA data retrieved from the cBioPortal platform.
e) Kaplan–Meier survival curve for gastric cancer cases, stratified by high versus low ESRP1 expression and assessed via log-rank testing.
f) Quantitative PCR measurement of ESRP1 (relative to GAPDH) in resected tumor samples from 24 gastric cancer patients; the dot plot compares levels in cases with versus without lymph node involvement (LNM vs. non-LNM).
g) Dot plot illustrating the inverse correlation between ESRP1 levels and lymph node ratio (LNR), accompanied by Pearson correlation analysis. LNR is derived as the ratio of involved lymph nodes to total nodes examined. *P < 0.05.

ESRP1 suppresses metastatic behavior in gastric cancer cells both in vitro and in vivo

To explore ESRP1's impact on gastric cancer dissemination, we generated stable ESRP1-overexpressing lines using SGC7901 and BGC823 cells, which exhibit baseline low ESRP1. Transwell assays revealed marked reductions in migratory and invasive abilities upon ESRP1 elevation **(Figures 2a and 2b).** Key EMT markers showed upregulation of E-cadherin and downregulation of N-cadherin following ESRP1 overexpression, indicating potential suppression of the EMT pathway **(Figure 2c).** In vivo validation via tail vein injection in mice demonstrated fewer pulmonary metastatic foci in the ESRP1-overexpressing cohort compared to controls **(Figures 2d–2f).** Immunohistochemical staining of lung sections further confirmed enhanced E-cadherin in metastatic lesions from the ESRP1-elevated group **(Figure 2g).**

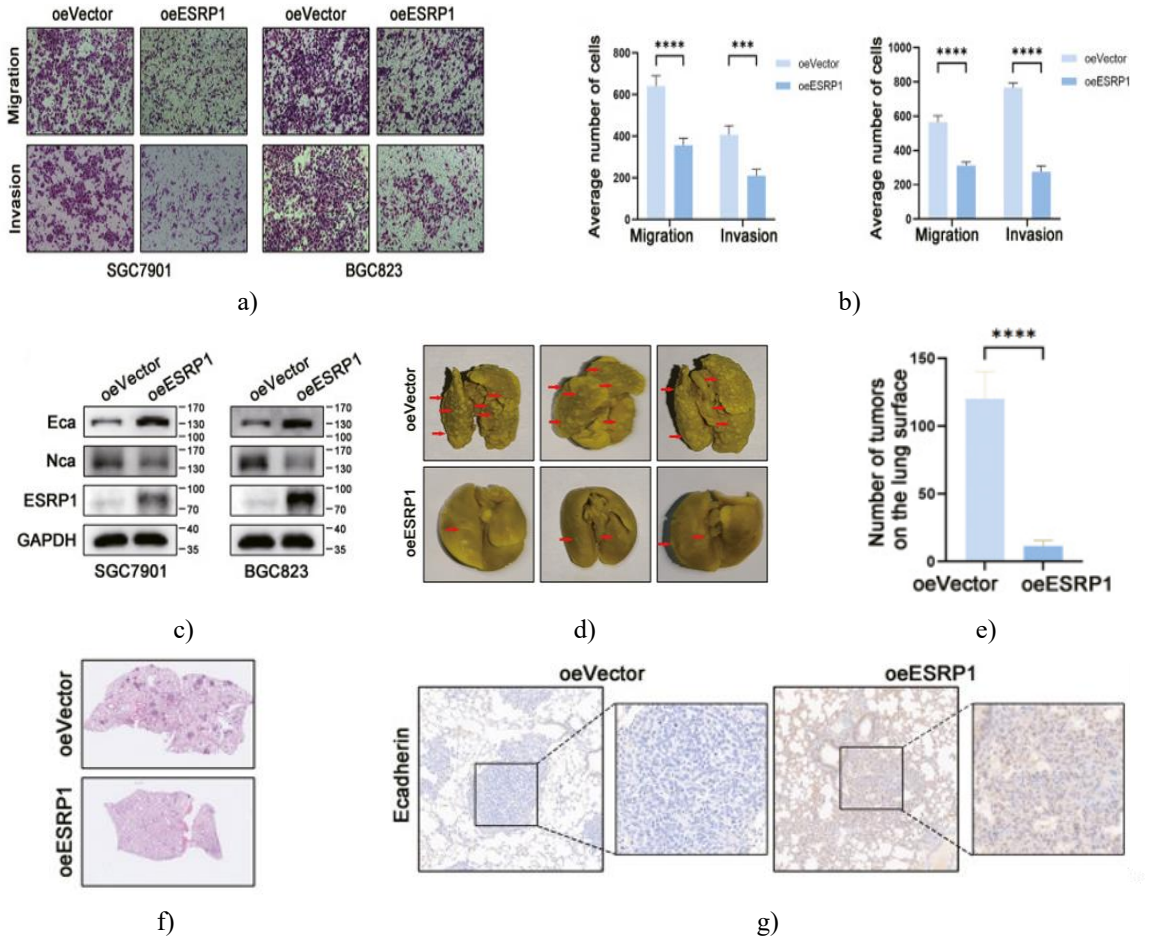

Figure 2. Elevation of ESRP1 restrains migratory and invasive properties of gastric cancer cells in laboratory and animal models.

a) Transwell assays evaluating migration and invasion in control (oeVector) and ESRP1-overexpressing (oeESRP1) gastric cancer cells. Left panels correspond to SGC7901 cells; right panels to BGC823 cells.

b) Bar graphs quantifying the number of cells that migrated or invaded through the membrane in Transwell assays. Left: SGC7901 cells; right: BGC823 cells.

c) Western blot analysis of E-cadherin, N-cadherin, ESRP1, and GAPDH protein levels in control (oeVector) and ESRP1-overexpressing (oeESRP1) cells. Left: SGC7901 cells; right: BGC823 cells.

d) In vivo assessment of ESRP1 overexpression on gastric cancer metastasis. 1×10^6 oeVector or oeESRP1 SGC7901 cells were administered via tail vein injection (n = 5 per group). After 1.5 months, mice were euthanized, and lungs were harvested and fixed in Bouin's solution. Representative lung images are displayed, with red arrows marking metastatic nodules.

e) Quantification of visible metastatic nodules on the lung surface, comparing oeVector and oeESRP1 groups.

f) Representative hematoxylin and eosin (H&E) stained sections of lungs from mice injected with oeVector or oeESRP1 SGC7901 cells.

g) Representative immunohistochemical staining for E-cadherin in pulmonary metastatic lesions. Left: oeVector group; right: oeESRP1 group.

*P < 0.05, **P < 0.01, ***P < 0.001, ****P < 0.0001.

Following ESRP1 depletion, AGS and MKN45 cells exhibited enhanced migratory and invasive capabilities in Transwell assays **(Figures 3a and 3b),** accompanied by reduced E-cadherin and elevated N-cadherin levels **(Figures 3c),** indicative of mesenchymal transition. This was substantiated by a higher number of pulmonary metastatic foci in mice receiving MKN45 cells with ESRP1 knockdown (**Figures 3d–3f)** and diminished E-cadherin expression within those metastases **(Figure 3g).** Together, these findings establish that ESRP1 suppresses metastatic progression in gastric cancer cells.

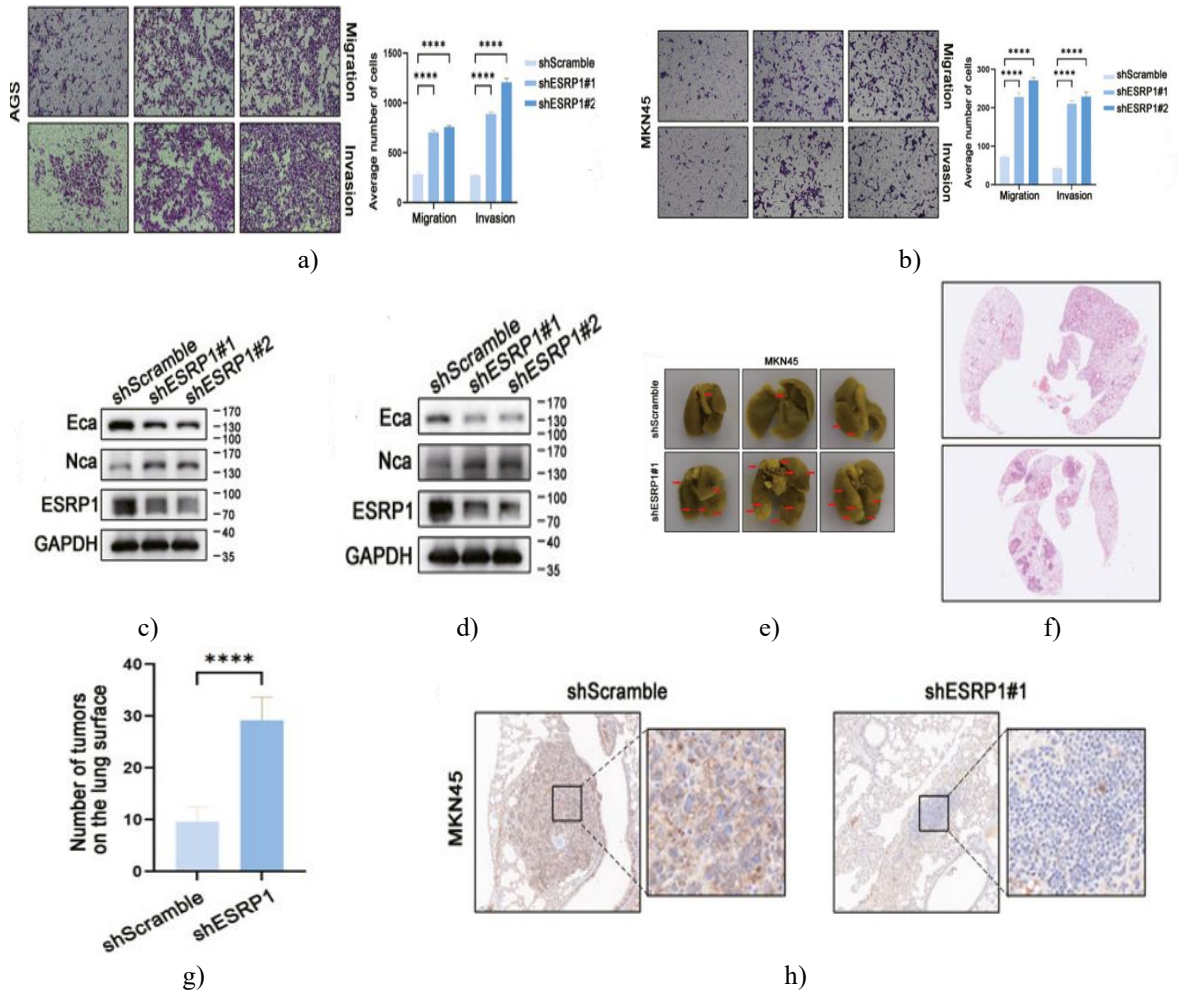

Figure 3. Depletion of ESRP1 enhances migratory and invasive properties of gastric cancer cells in vitro and in animal models.

a) Transwell assays assessing migration and invasion in AGS cells with control knockdown (shScramble) versus ESRP1 knockdown (shESRP1#1 and shESRP1#2). Left panels show representative images of migrated/invaded cells; right panels display corresponding quantification bar graphs.

b) Transwell migration and invasion assays in MKN45 cells with shScramble control versus shESRP1#1 and shESRP1#2 knockdown. Left panels present representative images; right panels show the associated statistical bar graphs.

c, d) Western blot examination of E-cadherin, N-cadherin, ESRP1, and GAPDH protein levels in ESRP1-depleted AGS cells (C) or MKN45 cells (D).

e) In vivo evaluation of metastatic capacity using MKN45 cells with shScramble or shESRP1#1. A total of 1 × 10^6 cells were introduced via tail vein injection (n = 5 per group). After 1.5 months, mice were euthanized, and lungs were harvested and fixed in Bouin's solution. Representative whole-lung images are shown.

f) Representative photographs of excised lungs from mice injected with MKN45 shScramble or shESRP1#1 cells.

g) Bar graph quantifying the number of surface metastatic nodules on lungs.

h) Representative immunohistochemical staining for E-cadherin in pulmonary metastatic lesions. Left: shScramble group; right: shESRP1#1 group.

****P < 0.0001.

ESRP1 modulates cell adhesion and induces extensive alternative splicing events

To elucidate the molecular pathways through which ESRP1 restrains gastric cancer metastasis, we conducted RNA sequencing on SGC7901 cells overexpressing ESRP1 compared to vector controls **(Figure 4a).** This analysis uncovered 3268 differentially expressed genes (DEGs), comprising 1684 upregulated and 1584 downregulated transcripts in ESRP1-overexpressing cells **(Figure 4b).** Gene Ontology (GO) enrichment of the

downregulated DEGs revealed prominent associations with cell adhesion processes **(Figure 4c),** whereas upregulated genes were predominantly linked to the extracellular region.

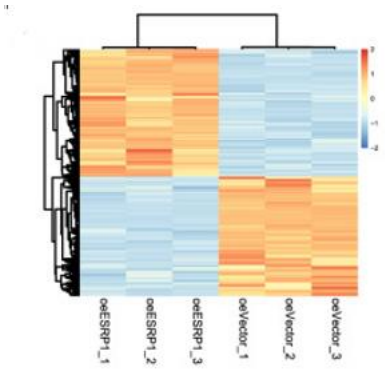

a)

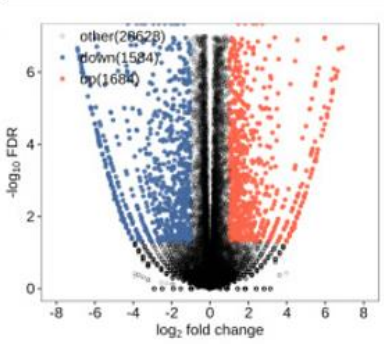

b)

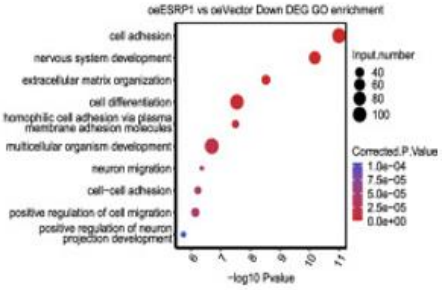

c)

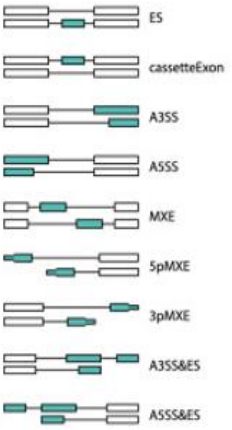

d)

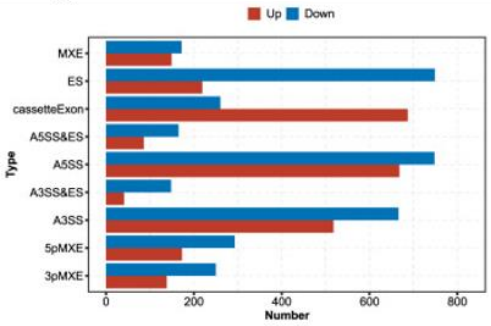

e)

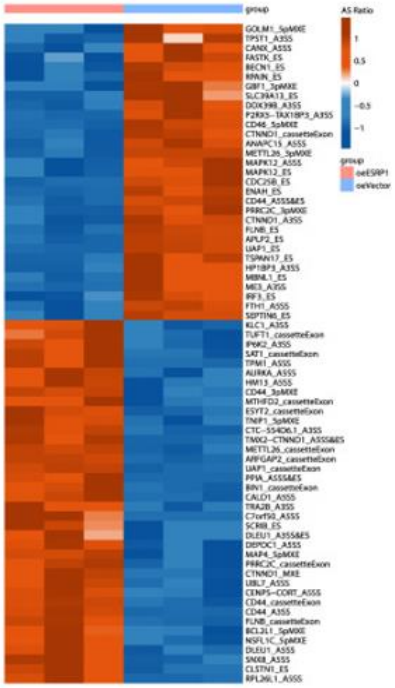

f)

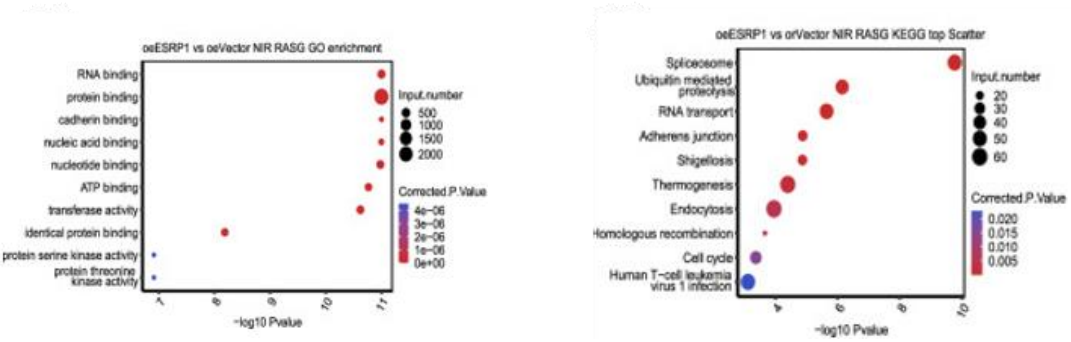

g) h)

Figure 4. ESRP1 triggers widespread alternative splicing alterations in gastric cancer cells.
a) Heatmap illustrating differentially expressed genes (DEGs) between control (oeVector) and ESRP1-overexpressing (oeESRP1) SGC7901 cells based on RNA sequencing data.
b) Volcano plot highlighting upregulated and downregulated DEGs identified through RNA sequencing.
c) Gene Ontology (GO) enrichment analysis performed on downregulated DEGs in oeESRP1 gastric cancer cells.
d) Illustrative schematic of common alternative splicing categories. ES: exon skipping; A3SS: alternative 3′ splice site; A5SS: alternative 5′ splice site; MXE: mutually exclusive exons; 5pMXE: MXE combined with alternative 5′ promoter; 3pMXE: MXE combined with alternative polyadenylation site.
e) Bar graph depicting the distribution and counts of various alternative splicing types.
f) Heatmap displaying the most prominent alternative splicing (AS) events in oeESRP1 SGC7901 cells. Events were selected based on splicing counts exceeding 50 and an absolute difference in AS ratio between groups greater than 0.2. Color scale represents the AS ratio.
g) GO enrichment analysis of genes exhibiting differential alternative splicing in oeESRP1 SGC7901 cells.
h) Kyoto Encyclopedia of Genes and Genomes (KEGG) pathway analysis of genes with differential alternative splicing in oeESRP1 SGC7901 cells.

In mammalian cells, alternative splicing primarily encompasses nine major forms, including exon skipping (ES), cassette exons, A3SS, A5SS, and MXE, among others **(Figure 4d).** Detailed examination showed that ESRP1-driven splicing events predominantly involve ES, A5SS, and A3SS **(Figure 4e).** To assess ESRP1-induced splicing changes quantitatively, we determined alternative splicing ratios, and the most significant events are visualized in a heatmap **(Figure 4f).** GO analysis of genes affected by differential splicing revealed strong enrichment in RNA-binding functions **(Figure 4g),** whereas KEGG analysis pointed to associations with spliceosome activity **(Figure 4h).** These findings indicate that ESRP1 influences cell adhesion while triggering extensive alternative splicing alterations across the transcriptome.

ESRP1 binds to CLSTN1 Exon 5 and induces skipping of exon 11

Cross-linking immunoprecipitation (CLIP) and its derivatives have proven effective for mapping precise RNA–protein interactions in cultured cells, tissues, and whole organisms. To pinpoint direct RNA targets of ESRP1, we conducted CLIP-seq in ESRP1-overexpressing SGC7901 cells **(Figure 5a).** Binding sites were predominantly located in introns (36.01%) and coding sequences (CDS; 32.56%) **(Figure 5b).** A total of 9299 transcripts were found to interact with ESRP1, among which 2374 displayed alternative splicing events **(Figure 5c).** The predominant binding motif recognized by ESRP1 was ‘CUGUUG’ **(Figure 5d).** Given that RNA-seq identified marked increases in alternative splicing ratios for SCRIB and CLSTN1 upon ESRP1 overexpression **(Figure 4f),** we searched for matching motifs. A corresponding site was detected in exon 5 of CLSTN1 **(Figure 5e).** CLSTN1 is a member of the calsyntenin family within the cadherin superfamily. Direct binding of ESRP1 to CLSTN1 exon 5 was validated using RIP-PCR **(Figure 5f).** Integrated analysis of CLIP-seq and RNA-seq data revealed multiple ESRP1 binding peaks along CLSTN1 mRNA, with ESRP1 primarily promoting skipping of exon 11 **(Figure 5g).** Using primers flanking exon 11, we confirmed that ESRP1 overexpression in gastric cancer cells increased the shorter isoform (exon 11 skipped, 103 bp) while reducing the longer isoform (exon 11 included, 160 bp) **(Figure 5h).** This pattern was corroborated in clinical samples: PCR analysis of 24 gastric cancer tissues showed a positive correlation between CLSTN1 splicing ratio (CLSTN1-S/CLSTN1-F) and ESRP1 expression **(Figures 5i and 5j).**

Moreover, the CLSTN1 splicing ratio was significantly lower in patients with lymph node metastasis (LNM) than in those without **(Figure 5k).** Survival data from SpliceSeq and OncoSplicing databases indicated that stomach adenocarcinoma patients with lower percent spliced-in (PSI) values for CLSTN1 exon 11 exhibited improved overall survival compared to those with higher PSI **(Figure 5l).** Collectively, these data demonstrate that ESRP1 directly binds exon 5 of CLSTN1 to promote exon 11 skipping, an event associated with reduced lymph node metastasis risk and better prognosis.

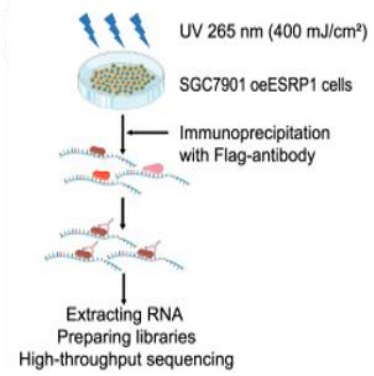

a)

b)

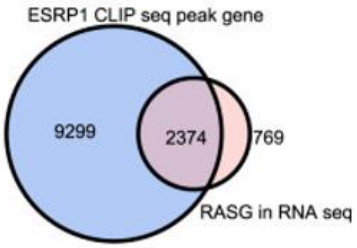

c)

d)

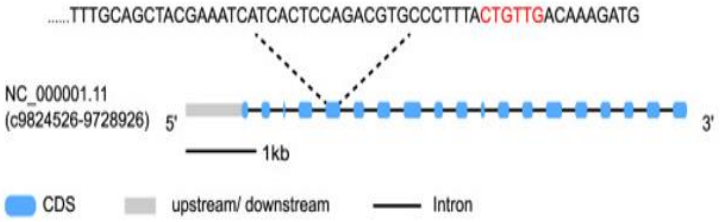

e)

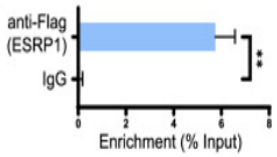

f)

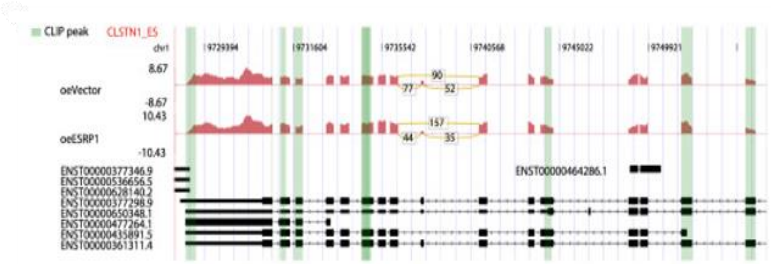

g)

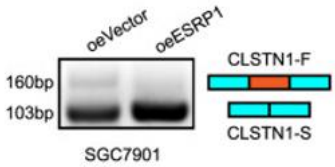

h)

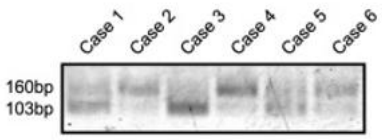

i)

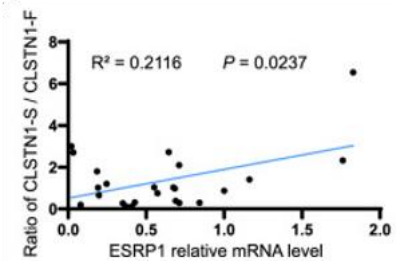

j)

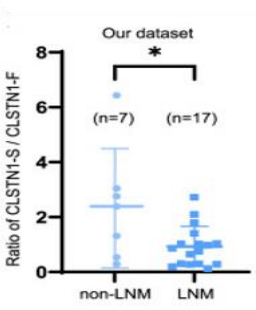

k)

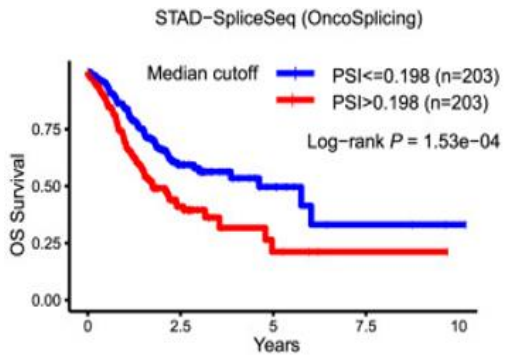

l)

Figure 5. ESRP1 facilitates skipping of exon 11 in CLSTN1.

a) Schematic overview of the CLIP-seq protocol. In brief, oeESRP1 SGC7901 gastric cancer cells were subjected to UV crosslinking at 400 mJ/cm², followed by cell lysis, immunoprecipitation using anti-Flag antibody, RNA isolation, library construction, and high-throughput sequencing.

b) Pie chart illustrating the genomic distribution of ESRP1 binding sites.

c) Venn diagram depicting the overlap between genes associated with ESRP1 binding peaks (from CLIP-seq) and genes exhibiting alternative splicing events (from RNA-seq).

d)Consensus binding motif recognized by ESRP1.

e) Schematic representation of the CLSTN1 genomic locus, with potential ESRP1 binding sites highlighted in red.

f) RIP-PCR validation confirming ESRP1 interaction with the exon 5 region of CLSTN1 mRNA in oeESRP1 SGC7901 cells.

g) Integrated view of RNA-seq read coverage across CLSTN1, with CLIP-seq binding peaks indicated by green lines.

h) Representative agarose gel images showing PCR products for the full-length (CLSTN1-F, exon 11 included) and spliced (CLSTN1-S, exon 11 skipped) isoforms in oeVector and oeESRP1 SGC7901 cells.

i) Representative agarose gel images of CLSTN1-F and CLSTN1-S PCR products from clinical gastric cancer specimens.

j) Scatter plot demonstrating the positive correlation between CLSTN1 splicing ratio (CLSTN1-S/CLSTN1-F) and ESRP1 expression levels in 24 gastric cancer samples. Splicing ratio was quantified via densitometry of gel bands; ESRP1 expression was measured by qPCR.

k) Comparison of CLSTN1 splicing ratios between gastric cancer patients with (LNM) and without (non-LNM) lymph node metastasis.

l) Kaplan–Meier survival curve illustrating the association between CLSTN1 percent spliced-in (PSI) values and overall survival in TCGA stomach adenocarcinoma patients, based on SpliceSeq data from the OncoSplicing database.

*P < 0.05.

CLSTN1 exon 11 splicing underlies esrp1-mediated suppression of gastric cancer metastasis

To investigate CLSTN1's contribution to gastric cancer metastasis, we generated overexpression constructs for the full-length isoform (CLSTN1-F) and the truncated isoform (CLSTN1-S) **(Figure 6a).** Transwell assays revealed that CLSTN1-S overexpression markedly impaired cell migration and invasion, whereas CLSTN1-F overexpression enhanced these properties **(Figure 6b).** Analysis of EMT markers showed that CLSTN1-S increased E-cadherin while decreasing N-cadherin protein levels, with CLSTN1-F producing the opposite effects **(Figure 6c)**, indicating that the short isoform likely drives ESRP1-dependent metastatic suppression.

To directly test this, we specifically depleted CLSTN1-S (oeES-shCL-S) in ESRP1-overexpressing cells **(Figure 6d)**. Rescue experiments demonstrated that reducing CLSTN1-S largely abrogated the inhibitory effects of ESRP1 on migration and invasion **(Figure 6e).** Moreover, oeES-shCL-S cells displayed reduced E-cadherin and elevated N-cadherin compared to oeESRP1 alone **(Figure 6f)**, consistent with induction of EMT. In vivo validation involved tail vein injection of the three cell groups into mice, with lung metastases assessed after one month. Depletion of CLSTN1-S substantially reversed the ESRP1-induced decrease in pulmonary metastatic burden **(Figures 6g–6i)**. Immunohistochemistry confirmed that ESRP1 overexpression upregulated E-cadherin in

metastatic lesions, an effect attenuated by CLSTN1-S knockdown **(Figure 6j).** These findings establish that the CLSTN1 short isoform is essential for ESRP1's antimetastatic activity in gastric cancer.

a)

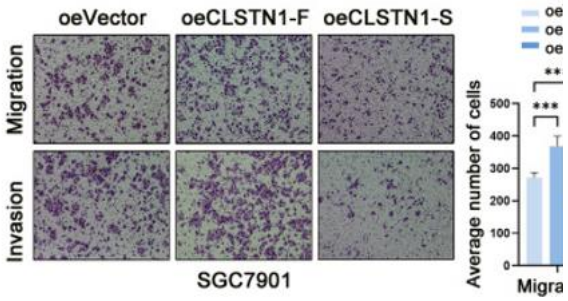

b)

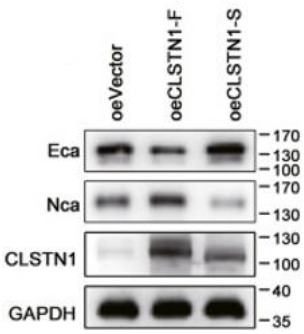

c)

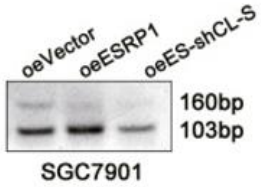

d)

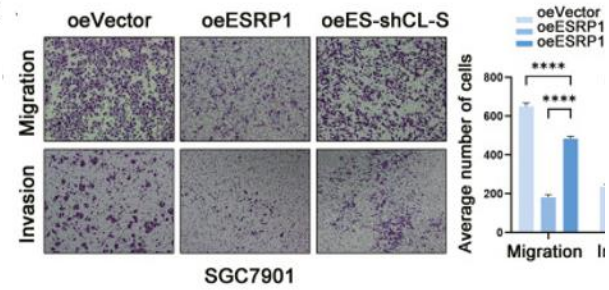

e)

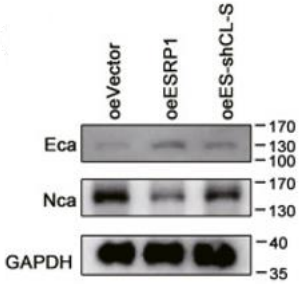

f)

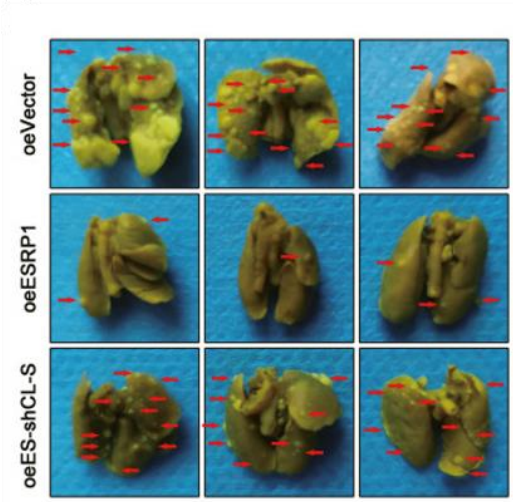

g)

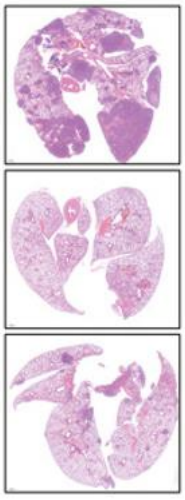

h)

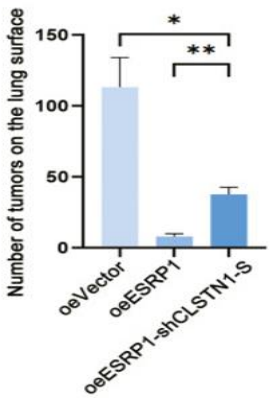

i)

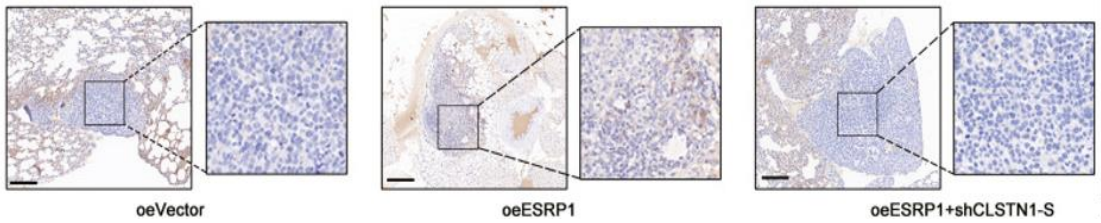

j)

Figure 6. Skipping of CLSTN1 exon 11 is required for ESRP1-driven suppression of gastric cancer cell metastasis.

a) Representative agarose gel images showing PCR products for CLSTN1 isoforms in SGC7901 cells with control vector (oeVector), full-length CLSTN1 overexpression (oeCLSTN1-F), or truncated CLSTN1 overexpression (oeCLSTN1-S).

b) Transwell assays evaluating migration and invasion in SGC7901 oeVector, oeCLSTN1-F, and oeCLSTN1-S cells. Left panels display representative images of migrated/invaded cells; right panels show corresponding quantification bar graphs.

c) Western blot analysis of E-cadherin (Eca), N-cadherin (Nca), CLSTN1, and GAPDH (GA) protein levels in SGC7901 oeVector, oeCLSTN1-F, and oeCLSTN1-S cells.

d) Representative agarose gel images of PCR products for CLSTN1 isoforms in SGC7901 cells with oeVector, oeESRP1, or oeESRP1 combined with CLSTN1-S knockdown (oeES-shCL-S).

e) Transwell migration and invasion assays in SGC7901 oeVector, oeESRP1, and oeES-shCL-S cells. Left panels present representative images; right panels provide the associated statistical bar graphs.

f) Western blot examination of E-cadherin (Eca), N-cadherin (Nca), and GAPDH protein levels in SGC7901 oeVector, oeESRP1, and oeES-shCL-S cells.

g) Photographs of lung surfaces from mice (n = 5 per group) injected via tail vein with SGC7901 oeVector, oeESRP1, or oeES-shCL-S cells. Lungs were fixed in Bouin's solution; red arrows mark metastatic nodules.

h) Representative hematoxylin and eosin (H&E) stained lung sections from the three groups. Top: oeVector; middle: oeESRP1; bottom: oeES-shCL-S.

i) Bar graph quantifying the number of surface metastatic nodules on lungs.

j) Representative immunohistochemical staining for E-cadherin in pulmonary metastatic lesions. Left: oeVector; middle: oeESRP1; right: oeES-shCL-S.

ns, not significant. *P < 0.05, **P < 0.01, ***P < 0.001, ****P < 0.0001.

CLSTN1 influences the stability of the E-cadherin/β-catenin adhesive complex

The binding between E-cadherin and β-catenin is critical for preserving cytoskeletal integrity and limiting cellular invasion and dissemination. To determine whether CLSTN1, as a member of the cadherin superfamily, participates in this interaction, we performed co-immunoprecipitation and detected endogenous association between CLSTN1 and β-catenin in gastric cancer cells **(Figure 7a).** Overexpression experiments revealed isoform-specific effects: CLSTN1-F increased β-catenin protein levels and weakened the E-cadherin–β-catenin interaction, whereas CLSTN1-S reduced β-catenin abundance and strengthened this binding **(Figure 7b).** Consistent with this, ESRP1 overexpression enhanced E-cadherin–β-catenin association while decreasing overall β-catenin protein in SGC7901 cells **(Figure 7c).** Immunofluorescence further supported these findings: ESRP1 elevation diminished β-catenin signal intensity but promoted its colocalization with E-cadherin at the plasma membrane **(Figure 7d).** Given that β-catenin is primarily degraded via the ubiquitin-proteasome pathway, we assessed degradation kinetics using cycloheximide (CHX) chase and observed accelerated β-catenin turnover upon ESRP1 overexpression **(Figure 7e).** Ubiquitination assays confirmed that both ESRP1 and CLSTN1-S enhanced β-catenin polyubiquitination, whereas CLSTN1-F suppressed it **(Figures 7f and 7g).** Collectively, these data indicate that CLSTN1-S exerts dual effects: it reinforces the E-cadherin–β-catenin adhesive complex to sustain cytoskeletal stability and cell–cell adhesion, while simultaneously facilitating β-catenin ubiquitination and proteasomal degradation. These mechanisms likely underlie ESRP1's suppression of gastric cancer metastasis via alternative splicing of CLSTN1.

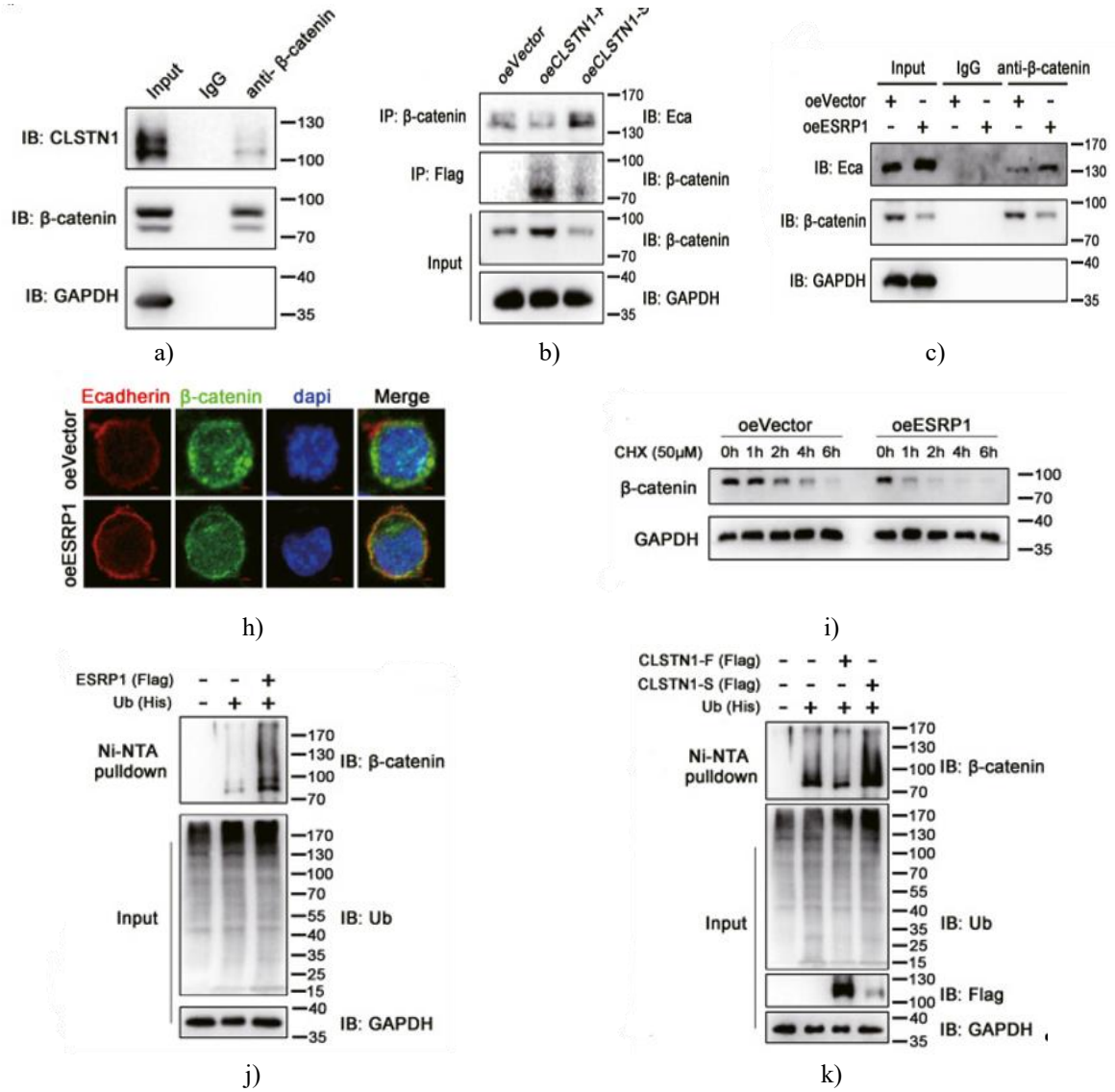

Figure 7. CLSTN1 modulates the E-cadherin–β-catenin interaction and complex stability.

a) Co-immunoprecipitation demonstrating interaction between endogenous CLSTN1 and β-catenin in SGC7901 gastric cancer cells. IB: immunoblotting.

b) Co-immunoprecipitation assessing interactions among β-catenin, E-cadherin, and the CLSTN1 isoforms in SGC7901 cells with control vector (oeVector), full-length CLSTN1 overexpression (oeCLSTN1-F), or truncated CLSTN1 overexpression (oeCLSTN1-S). IP: immunoprecipitation.

c) Co-immunoprecipitation examining the β-catenin–E-cadherin interaction in oeESRP1 SGC7901 cells.

d) Immunofluorescence analysis of β-catenin and E-cadherin colocalization in SGC7901 oeVector or oeESRP1 cells. Representative micrographs are presented.

e) Cycloheximide (CHX) chase assay evaluating β-catenin protein stability in SGC7901 oeVector or oeESRP1 cells.

f) Ni-NTA pulldown assay in HEK293T cells transfected with Flag-tagged ESRP1 and/or His-tagged ubiquitin plasmids.

g) Ni-NTA pulldown assay in HEK293T cells transfected with Flag-tagged CLSTN1-F, Flag-tagged CLSTN1-S, and/or His-tagged ubiquitin plasmids.

Gastric cancer remains a leading global malignancy with the fourth highest cancer-related mortality, primarily attributable to metastatic dissemination [1]. Alternative splicing represents a key mechanism generating protein isoform diversity and modulating numerous biological processes, including cellular invasion and motility [29–31]. Here, we established that the RNA-binding protein ESRP1 suppresses epithelial-mesenchymal transition (EMT) and metastatic spread in gastric cancer by driving skipping of exon 11 in CLSTN1 pre-mRNA. Clinical

validation further supported the prognostic value of ESRP1 expression and CLSTN1 splicing patterns, highlighting their potential utility for identifying patients at elevated metastatic risk and enabling timely intervention.

RNA-binding proteins (RBPs) constitute a vital cellular class that, via specialized RNA-interacting domains, orchestrate diverse post-transcriptional events such as splicing, localization, stability, editing, modification, and translation [32–34]. ESRP1 is a recognized RBP implicated in tumor metastasis, with prior evidence suggesting context-dependent roles—often opposing effects in reproductive versus gastrointestinal malignancies. In gastric cancer, earlier work demonstrated ESRP1-mediated promotion of LRRFIP2 exon 7 inclusion to restrain migration and invasion [22]. Building on this, our CLIP-seq analyses uncovered an additional pathway whereby ESRP1-dependent skipping of CLSTN1 exon 11 critically contributes to limiting invasive and metastatic behavior in gastric cancer.

Calsyntenin-1 (CLSTN1), a type I transmembrane protein within the cadherin superfamily, functions as a distinctive calcium-dependent linker between extracellular proteolysis and intracellular signaling [35]. Predominantly expressed in neuronal tissues, its roles in neoplasia have been underexplored [36, 37]. Known functions encompass cell adhesion and proliferation, and an N-glycosylation site within the alternatively spliced exon 11 implies functional divergence between full-length (CLSTN1-F) and short (CLSTN1-S) isoforms. We showed that the exon 11-skipped isoform (CLSTN1-S) potently curbs gastric cancer cell migration and invasion, and its targeted depletion abrogates ESRP1-conferred antimetastatic effects. This aligns with prior observations that CLSTN1 isoform switching governs EMT in breast cancer [38].

Metastasis involves a multifaceted cascade intertwined with processes like EMT, extracellular matrix remodeling, and angiogenesis [39–41]. EMT entails epithelial cells acquiring mesenchymal traits, marked by reduced E-cadherin and elevated N-cadherin expression [41, 42]. This transition is governed by numerous pathways, prominently including Wnt/β-catenin signaling [43]. β-catenin serves as a junctional scaffold bridging E-cadherin to the actin cytoskeleton, thereby reinforcing adherens junctions [44, 45]. Wnt activation stabilizes cytoplasmic β-catenin, facilitating its nuclear translocation and transcriptional activation of targets such as matrix metalloproteinase-7 (MMP-7) [46, 47]. Our findings reveal that ESRP1-orchestrated CLSTN1 exon 11 skipping elevates E-cadherin, thereby countering EMT in gastric cancer cells. Moreover, CLSTN1-S enhances E-cadherin–β-catenin binding, suggesting reinforced membrane-associated adherens junctions. These dual actions likely represent central mechanisms through which ESRP1 and CLSTN1-S impede metastatic progression.

Certain limitations warrant acknowledgment. We did not examine impacts of ESRP1 or CLSTN1-S on β-catenin nuclear shuttling or transcriptional activity, nor did we delineate precise pathways by which CLSTN1-S upregulates E-cadherin while downregulating N-cadherin—areas requiring future investigation. Nonetheless, this work furnishes novel mechanistic insights into ESRP1-driven suppression of gastric cancer invasion and dissemination.

Conclusion

In summary, we substantiated inverse associations between ESRP1 expression, CLSTN1 splicing ratios, and metastatic propensity across in vitro, in vivo, and patient-derived analyses. ESRP1 promotes generation of the short CLSTN1 isoform, which attenuates tumor cell EMT and fortifies the E-cadherin/β-catenin adhesive complex—a pivotal antimetastatic axis. These discoveries deepen understanding of the ESRP1–CLSTN1 regulatory network in gastric cancer metastasis and may inform innovative approaches for preventing or treating disseminated disease.

Acknowledgments: None

Conflict of Interest: None

Financial Support: None

Ethics Statement: None

References

1. Sung H, Ferlay J, Siegel RL, Laversanne M, Soerjomataram I, Jemal A, et al. Global Cancer Statistics 2020: GLOBOCAN Estimates of Incidence and Mortality Worldwide for 36 Cancers in 185 Countries. Ca: A Cancer J Clinicians. 2021;71:209–49. doi: 10.3322/caac.21660.
2. Wong MCS, Huang J, Chan PSF, Choi P, Lao XQ, Chan SM, et al. Global incidence and mortality of gastric cancer, 1980-2018. Jama Netw Open. 2021;4:e2118457. doi: 10.1001/jamanetworkopen.2021.18457.
3. Muro K, Van Cutsem E, Narita Y, Pentheroudakis G, Baba E, Li J, et al. Pan-Asian adapted ESMO Clinical Practice Guidelines for the management of patients with metastatic gastric cancer: a JSMO-ESMO initiative endorsed by CSCO, KSMO, MOS, SSO and TOS. Ann Oncol. 2019;30:19–33. doi: 10.1093/annonc/mdy502.
4. Van Cutsem E, Sagaert X, Topal B, Haustermans K, Prenen H. Gastric cancer. Lancet. 2016;388:2654–64. doi: 10.1016/S0140-6736(16)30354-3.
5. Hong S. RNA binding protein as an emerging therapeutic target for cancer prevention and treatment. J Cancer Prev. 2017;22:4:203–10. doi: 10.15430/JCP.2017.22.4.203.
6. Hentze MW, Castello A, Schwarzl T, Preiss T. A brave new world of RNA-binding proteins. Nat Rev Mol Cell Biol. 2018;19:327–41. doi: 10.1038/nrm.2017.130.
7. Moore, Purcaro JE, Pratt HE MJ, Epstein CB, Shoresh N, Adrian J, et al. Expanded encyclopaedias of DNA elements in the human and mouse genomes. Nature. 2020;583:699–710. doi: 10.1038/s41586-020-2493-4.
8. Zhang P, Abdelmohsen K, Liu Y, Tominaga-Yamanaka K, Yoon J, Ioannis G, et al. Novel RNA- and FMRP-binding protein TRF2-S regulates axonal mRNA transport and presynaptic plasticity. Nat Commun. 2015;6:8888. doi: 10.1038/ncomms9888.
9. Mushtaq A, Mir US, Altaf M. Multifaceted functions of RNA-binding protein vigilin in gene silencing, genome stability, and autism-related disorders. J Biol Chem. 2023;299:102988. doi: 10.1016/j.jbc.2023.102988.
10. Tang J, He J, Guo H, Lin H, Li M, Yang T, et al. PTBP2-mediated alternative splicing of IRF9 controls tumor-associated monocyte/macrophage chemotaxis and repolarization in neuroblastoma progression. Research. 2023;6:33. doi: 10.34133/research.0033.
11. Warzecha CC, Carstens RP. Complex changes in alternative pre-mRNA splicing play a central role in the epithelial-to-mesenchymal transition (EMT). Semin Cancer Biol. 2012;22:417–27. doi: 10.1016/j.semcancer.2012.04.003.
12. Gao H, Wei H, Yang Y, Li H, Liang J, Ye J, et al. Phase separation of DDX21 promotes colorectal cancer metastasis via MCM5-dependent EMT pathway. Oncogene. 2023;42:1704–15. doi: 10.1038/s41388-023-02687-6.
13. Liu W, Li D, Lu T, Zhang H, Chen Z, Ruan Q, et al. Comprehensive analysis of RNA-binding protein SRSF2-dependent alternative splicing signature in malignant proliferation of colorectal carcinoma. J Biol Chem. 2023;299:102876. doi: 10.1016/j.jbc.2023.102876.
14. Göttgens E, Span PN, Zegers MM. Roles and regulation of epithelial splicing regulatory proteins 1 and 2 in epithelial-mesenchymal transition. Int Rev Cel Mol Biol. 2016;327:163–94. doi: 10.1016/bs.ircmb.2016.06.003.
15. Wang W, Taufalele PV, Millet M, Homsy K, Smart K, Berestesky ED, et al. Matrix stiffness regulates tumor cell intravasation through expression and ESRP1-mediated alternative splicing of MENA. Cell Rep. 2023;42:112338. doi: 10.1016/j.celrep.2023.112338.
16. Ueda J, Matsuda Y, Yamahatsu K, Uchida E, Naito Z, Korc M, et al. Epithelial splicing regulatory protein 1 is a favorable prognostic factor in pancreatic cancer that attenuates pancreatic metastases. Oncogene. 2014;33:4485–95. doi: 10.1038/onc.2013.392.
17. Li L, Qi L, Qu T, Liu C, Cao L, Huang Q, et al. Epithelial splicing regulatory protein 1 inhibits the invasion and metastasis of lung adenocarcinoma. Am J Pathol. 2018;188:1882–94. doi: 10.1016/j.ajpath.2018.04.012.
18. Yae T, Tsuchihashi K, Ishimoto T, Motohara T, Yoshikawa M, Yoshida GJ, et al. Alternative splicing of CD44 mRNA by ESRP1 enhances lung colonization of metastatic cancer cell. Nat Commun. 2012;3:883. doi: 10.1038/ncomms1892.

19. Chen L, Yao Y, Sun L, Zhou J, Miao M, Luo S, et al. Snail driving alternative splicing of CD44 by ESRP1 enhances invasion and migration in epithelial ovarian cancer. Cell Physiol Biochem. 2017;43:2489–504. doi: 10.1159/000484458.
20. Freytag M, Kluth M, Bady E, Hube-Magg C, Makrypidi-Fraune G, Heinzer H, et al. Epithelial splicing regulatory protein 1 and 2 (ESRP1 and ESRP2) upregulation predicts poor prognosis in prostate cancer. Bmc Cancer. 2020;20:1220. doi: 10.1186/s12885-020-07682-8.
21. Teles SP, Oliveira P, Ferreira M, Carvalho J, Ferreira P, Oliveira C. Integrated analysis of structural variation and RNA expression of FGFR2 and its splicing modulator ESRP1 highlight the ESRP1(amp)-FGFR2(norm)-FGFR2-IIIc(high) axis in diffuse gastric cancer. Cancers. 2019;12:70. doi: 10.3390/cancers12010070.
22. Lee J, Pang K, Kim J, Hong E, Lee J, Cho HJ, et al. ESRP1-regulated isoform switching of LRRFIP2 determines metastasis of gastric cancer. Nat Commun. 2022;13:6274. doi: 10.1038/s41467-022-33786-9.
23. Rinn JL, Kertesz M, Wang JK, Squazzo SL, Xu X, Brugmann SA, et al. Functional demarcation of active and silent chromatin domains in human HOX loci by noncoding RNAs. Cell. 2007;129:1311–23. doi: 10.1016/j.cell.2007.05.022.
24. Khalil AM, Guttman M, Huarte M, Garber M, Raj A, Rivea Morales D, et al. Many human large intergenic noncoding RNAs associate with chromatin-modifying complexes and affect gene expression. Proc Natl Acad Sci USA. 2009;106:11667–72. doi: 10.1073/pnas.0904715106.
25. Cerami E, Gao J, Dogrusoz U, Gross BE, Sumer SO, Aksoy BA, et al. The cBio cancer genomics portal: an open platform for exploring multidimensional cancer genomics data. Cancer Discov. 2012;2:401–4. doi: 10.1158/2159-8290.CD-12-0095.
26. Lánczky A, Győrffy B. Web-based survival analysis tool tailored for medical research (KMplot): development and implementation. J Med Internet Res. 2021;23:e27633. doi: 10.2196/27633.
27. Ryan M, Wong WC, Brown R, Akbani R, Su X, Broom B, et al. TCGASpliceSeq: a compendium of alternative mRNA splicing in cancer. Nucleic Acids Res. 2016;44:D1018–22. doi: 10.1093/nar/gkv1288.
28. Zhang Y, Yao X, Zhou H, Wu X, Tian J, Zeng J, et al. OncoSplicing: an updated database for clinically relevant alternative splicing in 33 human cancers. Nucleic Acids Res. 2022;50:D1340–7. doi: 10.1093/nar/gkab851.
29. Choi S, Cho N, Kim KK. The implications of alternative pre-mRNA splicing in cell signal transduction. Exp Mol Med. 2023;55:755–66. doi: 10.1038/s12276-023-00981-7.
30. Fackenthal JD. Alternative mRNA splicing and promising therapies in cancer. Biomolecules. 2023;13.
31. Kretova M, Selicky T, Cipakova I, Cipak L. Regulation of pre-mRNA splicing: indispensable role of post-translational modifications of splicing factors. Life. 2023;13:604. doi: 10.3390/life13030604.
32. Bertoldo JB, Müller S, Hüttelmaier S. RNA-binding proteins in cancer drug discovery. Drug Discov Today. 2023;28:103580. doi: 10.1016/j.drudis.2023.103580.
33. Cen Y, Chen L, Liu Z, Lin Q, Fang X, Yao H, et al. Novel roles of RNA-binding proteins in drug resistance of breast cancer: from molecular biology to targeting therapeutics. Cell Death Discov. 2023;9:52. doi: 10.1038/s41420-023-01352-x.
34. Gao Y, Cao H, Huang D, Zheng L, Nie Z, Zhang S. RNA-binding proteins in bladder cancer. Cancers. 2023;15:1150. doi: 10.3390/cancers15041150.
35. Rindler MJ, Xu C, Gumper I, Cen C, Sonderegger P, Neubert TA. Calsyntenins are secretory granule proteins in anterior pituitary gland and pancreatic islet alpha cells. J Histochem Cytochem. 2008;56:381–8. doi: 10.1369/jhc.7A7351.2007.
36. Cheng K, Chen Y, Yue C, Zhang S, Pei Y, Cheng G, et al. Calsyntenin-1 negatively regulates ICAM5 accumulation in postsynaptic membrane and influences dendritic spine maturation in a mouse model of Fragile X Syndrome. Front Neurosci. 2019;13:1098. doi: 10.3389/fnins.2019.01098.
37. Ou M, Xiao Q, Ju X, Zeng P, Huang J, Sheng A, et al. The CTNNBIP1-CLSTN1 fusion transcript regulates human neocortical development. Cell Rep. 2021;35:109290. doi: 10.1016/j.celrep.2021.109290.
38. Hu X, Harvey SE, Zheng R, Lyu J, Grzeskowiak CL, Powell E, et al. The RNA-binding protein AKAP8 suppresses tumor metastasis by antagonizing EMT-associated alternative splicing. Nat Commun. 2020;11:486. doi: 10.1038/s41467-020-14304-1.
39. Yilmaz M, Christofori G, Lehembre F. Distinct mechanisms of tumor invasion and metastasis. Trends Mol Med. 2007;13:535–41. doi: 10.1016/j.molmed.2007.10.004.

40. Azadi S, Tafazzoli Shadpour M. The microenvironment and cytoskeletal remodeling in tumor cell invasion. Int Rev Cell Mol Biol. 2020;356:257–89. doi: 10.1016/bs.ircmb.2020.06.003.
41. Ang HL, Mohan CD, Shanmugam MK, Leong HC, Makvandi P, Rangappa KS, et al. Mechanism of epithelial-mesenchymal transition in cancer and its regulation by natural compounds. Med Res Rev. 2023;43:1141–200. doi: 10.1002/med.21948.
42. Yin Y, Liu W, Shen Q, Zhang P, Wang L, Tao R, et al. The DNA endonuclease Mus81 regulates ZEB1 expression and serves as a target of BET4 inhibitors in gastric cancer. Mol Cancer Ther. 2019;18:1439–50. doi: 10.1158/1535-7163.MCT-18-0833.
43. Zhang J, Hu Z, Horta CA, Yang J. Regulation of epithelial-mesenchymal transition by tumor microenvironmental signals and its implication in cancer therapeutics. Semin Cancer Biol. 2023;88:46–66. doi: 10.1016/j.semcancer.2022.12.002.
44. Takeichi M. Dynamic contacts: rearranging adherens junctions to drive epithelial remodelling. Nat Rev Mol Cell Biol. 2014;15:397–410. doi: 10.1038/nrm3802.
45. Katoh M. Multi-layered prevention and treatment of chronic inflammation, organ fibrosis and cancer associated with canonical WNT/β-catenin signaling activation (Review). Int J Mol Med. 2018;42:713–25. doi: 10.3892/ijmm.2018.3689.
46. Chen D, Feng Y, Cao G, Zhao Y. Natural products as a source for antifibrosis therapy. Trends Pharm Sci. 2018;39:937–52. doi: 10.1016/j.tips.2018.09.002.
47. Chen D, Wu X, Chen L, Hu H, Wang Y, Zhao Y. Poricoic acid A as a modulator of TPH-1 expression inhibits renal fibrosis via modulating protein stability of β-catenin and β-catenin-mediated transcription. Ther Adv Chronic Dis. 2020;11:1754254424. doi: 10.1177/2040622320962648.